Article

Journal of Vibration and Control
2014, Vol. 20(12) 1783–1795

DOI: 10.1177/1077546312475150
jvc.sagepub.com

Intelligent damage identification method for large structures based on strain modal parameters

Longjun He, Jijian Lian and Bin Ma

Abstract

Early damage detection not only improves the safety and reliability of structures but also reduces maintenance cost. However, damage detection is difficult to implement in large structures under ambient excitation because of the limitation of sensors, the uncertainty of ambient excitation, and the global properties of modal frequencies and displacement modes. This paper proposes a new damage detection method that employs the real encoding multi-swarm particle swarm optimization algorithm and fitness functions evolved from strain modes to find the optimal match between measured and simulated modal parameters and to determine the actual condition of structures. The proposed method requires low-frequency modes and incomplete modes and does not require mass normalization of parameters, thus making the method suitable for nondestructive dynamic damage detection of large structures under ambient excitation. Taking a concrete guide wall structure as an example, this paper studied the global searching performance and the sensitivity of the proposed method. The efficiency of the proposed method was analyzed by using different noise levels and sensor numbers. Results show that the proposed method is effective and can be applied in many types of large structures.

Keywords

Damage detection, strain mode, particle swarm optimization algorithm, ambient excitation, large structure, optimal sensor placement

1. Introduction

Damage detection methods can be classified into four levels according to the level of identification attempted: Level 1, detecting the presence of damage in the structure; Level 2, determination of the geometric location of the damage; Level 3, quantification of the severity of the damage; Level 4, prediction of the remaining lifespan of the structure (Doebling et al., 1998). In recent years, damage detection methods that are based on modal information changes have generated a wide concern in the fields of civil engineering, hydraulic engineering, mechanical engineering, and aerospace engineering (Fritzen and Jennewein, 1998; Cerri and Vestroni, 2003; Qian et al., 2008; Guo and Li, 2011). However, damage detection methods that are based on artificial incentives are difficult to implement and may not even be applicable for large structures. Therefore, damage diagnosis for structures under ambient excitation has attracted much attention in the research community. Structural damage can lead to changes in the physical properties of the structure (e.g., structural stiffness and damping) and may affect the dynamic properties of the structure (e.g., modal frequency and shape). Therefore, structural damage detection may be achieved by identifying structural dynamic parameters under the action of wind and flow (Li and Law, 2010). Displacement and acceleration are measured to determine the structural modal frequency and displacement

State Key Laboratory of Hydraulic Engineering Simulation and Safety, Tianjin University, Tianjin, People's Republic of China

Received: 9 September 2012; accepted: 14 December 2012

Corresponding author:
Jijian Lian, State Key Laboratory of Hydraulic Engineering Simulation and Safety, Tianjin University, Tianjin 300072, People's Republic of China.
Email: tjulianjj@163.com

mode of structures. However, only low frequencies and incomplete modes are obtained during the process because of excitation and limitation of sensors. Local damage is often neglected because of the global properties of modal frequency and displacement mode. Other signal processing methods, including wavelet transform (Hera and Hou, 2004; Hester and Gonzalez, 2012) and Hilbert–Huang transform (Huang and Shen, 1998; Tang et al., 2010), cannot essentially change the global properties of modal frequency and displacement mode. With the development of optical fiber measurement, structural damage detection by using strain modes has attracted extensive attention worldwide (Tsuda et al., 2004; Minakuchi et al., 2009). This type of measurement can obtain strain modes directly and can avoid errors caused by strain mode calculation using differences in displacement modes. The result shows that strain parameters, such as strain modes, are more sensitive to location damages in several simple structures (Li et al., 2002), and more requirements are needed for optimal sensor placement because of the local property of strain modes.

Model updating methods that are based on intelligent algorithms have recently attracted much attention in the damage detection field. Based on the optimization ability of the intelligent algorithms, these methods can simulate measured parameters and then determine the finite element (FE) model that can reflect the actual structure condition, which enables these methods to identify the locations and degrees of damage accurately. Damage detection methods have been reported to use algorithms, including the artificial neural network (ANN) (Wu et al., 1992; Parka et al., 2009), support vector machine (SVM) (Song et al., 2006; He and Yan, 2007), and genetic algorithm (GA) (Mares and Surace, 1996; He and Hwang, 2006; Gomes and Silva, 2008; Vakil-Baghmisheh et al., 2008; Meruane and Heylen, 2011). However, the ANN and SVM require neutral training, in which a large amount of data is demanded. By contrast, the GA and particle swarm optimization (PSO) algorithm, which are based on the laws of natural evolution and survival, do not rely on a large amount of data. One of the important characteristics of the GA and PSO algorithm is that these algorithms can seek for a global optimal solution by using multiple-point routes rather than single-point routes. Although the GA is a reliable tool for determining a global optimal solution, new intelligent optimization algorithms may further improve the optimization efficiency. The PSO algorithm, proposed by Kennedy and Eberhart (1995), shows strong vitality in solving nonlinear, nondifferentiable, and multi-peak optimization problems. The PSO algorithm has fast convergence, requires few parameters, is easy to implement, and utilizes a deep, intelligent background.

From these viewpoints, this study proposes a new damage detection method for large structures under ambient excitation. This damage detection method employs the real encoding multi-swarm particle swarm optimization (RMPSO) algorithm and the fitness functions evolved from strain modes to find the optimal match between measured and simulated modal parameters and to obtain actual structure conditions. Firstly, a new damage index, which is based on uniformly distributed strain mode shapes (SMSs) between measured points, is introduced to match the simulated data with the measured data. Secondly, the RMPSO algorithm is proposed to achieve the global optimum solution. The actual damage conditions can be effectively determined by updating the parameters of the FE model. Thirdly, a concrete guide wall structure with multiple damage scenarios provides an experimental framework for model verification. The sensor placement scheme was determined based on an optimal placement technique. The efficiency of the proposed damage detection method was evaluated by using damage cases with different noise levels and sensor numbers.

The rest of the paper is organized as follows. Section 2 presents four different fitness functions for damage detection, and Section 3 presents the proposed RMPSO algorithm for intelligent model updating. The proposed method was tested on a concrete guide wall structure for verification in Section 4, and Section 5 concludes the paper.

2. Damage detection procedure

Damage decreases the stiffness of structures. Therefore, structural damage is often simulated by decreasing a physical parameter, such as the elasticity module (E), cross-sectional area (A), and moment of inertia (I). In this study, damage degree is defined as the relative decrease in elasticity module and is expressed as follows:

$$\beta_i = \frac{E_i - E_i^d}{E_i} \times 100\%, \tag{1}$$

where β_i is the damage degree of the ith element, E_i is the initial elastic modulus of the ith element, and E_i^d is the current elastic modulus of the ith element. The value $\beta_i = 0$ indicates that the element is undamaged, whereas $0 < \beta_i \leq 1$ indicates that the element is partly or completely damaged.

If β_i is defined as an updating variable, then the problem of detecting damage becomes a constrained nonlinear optimization problem. The fitness function is expressed as the error between the measured and numerical modal data. However, only low frequencies,

low displacement mode shapes (DMSs), and low SMSs can be accurately obtained during the dynamic test for large structures under ambient excitation. Several structural parameters, such as stiffness matrices, mass matrices, and damping, are unavailable. The exciting forces for large structures are often hardly measured; thus, the mass-normalized factors are unknown, and the DMSs and SMSs are not normalized. Therefore, most damage detection methods for large structures under ambient excitation are only suitable for theoretical research, but not in practice.

To solve the aforementioned problem, this study considers four fitness functions to detect damage in large structures under ambient excitation. The first and third fitness functions were obtained from previous studies and then improved (Meruane and Heylen, 2011), whereas the second and fourth functions were first proposed in this paper.

(1) Error in frequency.

$$F_1(\{\beta\}) = \sum_{j=1}^{m} \left(\frac{\omega_{A,j}^2(\{\beta\})}{\omega_{E,j}^2} - 1 \right)^2. \tag{2}$$

Here, m is the number of measured modes; the subscripts A and E refer to analytical and experimental data, respectively; ω_j is the jth natural frequency. A small frequency error yields a small fitness value.

(2) Uniform distribution of ratios of DMSs. The values of measured and calculated modal shapes for the same structure and same order are probably not the same between measured points, and measured modal shapes in large structures under ambient excitation usually cannot be normalized. However, modal shapes must be uniformly distributed whether the modal shapes are normalized or not; that is, the ratios of the measured and calculated modal shapes with the same order are constant on measured points. The uniform distribution of the ratios of the measured and simulated DMSs is used as a fitness function to determine the agreement between actual and simulated modal information. The above fitness function is expressed as follows:

$$F_2(\{\beta\}) = \sum_{j=1}^{m} \sigma_j = \sum_{j=1}^{m} \left(\frac{1}{n-1} \sum_{i=1}^{n} \left(\frac{\phi_{E,ij}}{\phi_{A,ij}} - \frac{1}{n} \sum_{i=1}^{n} \frac{\phi_{E,ij}}{\phi_{A,ij}} \right)^2 \right)^{\frac{1}{2}}, \tag{3}$$

where n is the number of measured degrees of freedom (DOFs); m is the number of measured modes; ϕ_{ij} refers to the jth DMS on the ith measure point; $\phi_{E,ij}/\phi_{A,ij}$ refers to the ratios of measured and simulated DMSs; σ_j is the standard deviation of the scale vector of the jth measured and simulated DMSs and is used for estimating the uniformity of the ratios of measured and simulated DMSs distributed between measured points. The more uniform the distributed ratios are, the smaller the fitness of the objective function becomes.

(3) Correlation coefficient based on SMSs. The correlation coefficient between the jth measured and simulated SMS is defined as follows:

$$Cor_j = \frac{\left(\psi_{E,j}^T \cdot \psi_{A,j} \right)^2}{\left(\psi_{E,j}^T \cdot \psi_{E,j} \right) \left(\psi_{A,j}^T \cdot \psi_{A,j} \right)}, \quad j = 1, 2, \ldots, m, \tag{4}$$

where ψ_j is the jth SMS, and m is the number of measured modes.

Equation (4) shows that Cor_j represents the correlation between two modal shape vectors. According to the Cauchy–Schwarz Inequality

$$0 \le Cor_j \le 1. \tag{5}$$

The above inequality indicates that no correlation exists between two modal shapes when the correlation coefficient is equal to 0, whereas an upper limit of 1 denotes that two modal shapes are completely correlated. The third fitness function is introduced as follows:

$$F_3(\{\beta\}) = \sum_{j=1}^{m} (1 - Cor_j). \tag{6}$$

Thus

$$F_3(\{\beta\}) = \sum_{j=1}^{m} \left(1 - \frac{\left(\psi_{E,j}^T \cdot \psi_{A,j} \right)^2}{\left(\psi_{E,j}^T \cdot \psi_{E,j} \right) \left(\psi_{A,j}^T \cdot \psi_{A,j} \right)} \right). \tag{7}$$

According to the above equation, highly relevant measured and simulated SMSs yield smaller fitness values.

(4) Uniform distribution of the ratios of SMSs. According to the uniform distribution of the ratios of DMSs, the objective function for uniform distribution of the ratios of the measured and simulated SMSs is defined as follows:

$$F_4(\{\beta\}) = \sum_{j=1}^{m} \tau_j = \sum_{j=1}^{m} \left(\frac{1}{n-1} \sum_{i=1}^{n} \left(\frac{\psi_{E,ij}}{\psi_{A,ij}} - \frac{1}{n} \sum_{i=1}^{n} \frac{\psi_{E,ij}}{\psi_{A,ij}} \right)^2 \right)^{\frac{1}{2}}, \tag{8}$$

where ψ_{ij} represents the jth SMS on the ith measure point; $\psi_{E,ij}/\psi_{A,ij}$ refers to the ratios of measured and

simulated SMSs; τ_j is the standard deviation of the scale vector of the jth measured and simulated SMS and is used for estimating the uniformity of the ratios of measured and simulated SMSs distributed between measured points. The more uniform the distributed ratios are, the smaller the fitness of the objective function becomes.

The objective function E considers one of the above four fundamental functions and a damage penalization term. Thus

$$E_h(\{\beta\}) = F_h(\{\beta\}) + \gamma \sum_{k=1}^{n_E} \beta_k, \quad \forall h = 1, 2, 3, 4. \tag{9}$$

With the addition of the damage penalization term $\gamma \sum_{k=1}^{n_E} \beta_k$, the objective function can search not only the best correlation, but also the minimum possible damage. Thus, false damage detection caused by experimental noise or numerical errors can be avoided. The value of γ depends on the confidence in the numerical model and the experimental data.

The optimization problem is defined as follows:

$$\begin{aligned} &\text{Find} : X = \left[x_1, x_2, \ldots, x_{n_E}\right]^T \\ &\text{Minimize} : E(\{\beta\}) \\ &\text{Subject to} : 0 \le \beta_k \le 1, \end{aligned} \tag{10}$$

where n_E is the number of potential damage elements. The damage detection problem is transformed into a constraint nonlinear minimization problem by defining the objective function. The smaller the fitness function is, the more similar the information becomes. In this study, we propose the RMPSO algorithm to improve the global searching ability of existing intelligence algorithms.

3. Real encoding multi-swarm particle swarm optimization algorithm

3.1. Real encoding particle swarm optimization algorithm

PSO is a new swarm intelligence algorithm based on the stochastic optimization technique developed by Dr. Kennedy and Dr. Eberhart in 1995, inspired by the social behavior of bird flocking. PSO shares many similarities with evolutionary computation techniques, such as GAs. The system is initialized with a population of random solutions and searches for optima by updating generations. However, unlike GAs, the standard particle swarm optimization (SPSO) algorithm has no evolution operators, such as crossover and mutation.

SPSO can be expressed as follows: the potential solutions, called particles, fly through the problem space by following the current optimum particles. Each particle keeps track of its coordinates in the problem space that are associated with the best solution (fitness) it has achieved so far (the fitness value is also stored). This value is called "pbest". Another "best" value that is tracked by the particle swarm optimizer is the best value, obtained so far by any particle in the neighborhood of the particle. This location is called "lbest". When a particle takes all the population as its topological neighbors, the best value is a global best and is called "gbest". The PSO concept consists of, at each time step, changing the velocity of (accelerating) each particle toward its "pbest" and "gbest" locations. Acceleration is weighted by a random term, with separate random numbers being generated for acceleration toward "pbest" and "gbest" locations.

In this paper, the real encoding form is used in describing the solution domain to optimize simultaneously the damage location and degree. The number of potential damage elements is defined as the dimension of a particle, and the value in each dimension represents the damage degree of the corresponding element; that is, $x_{id} \in [0, 1]$. Here, $x_{id} = 0$ indicates that the element is undamaged, whereas $0 < x_{id} \le 1$ implies that the element has partial or complete damage. Taking a cantilever beam with 10 potential damage elements as an example, if the optimal solution is $[0, 0, 0.3, 0, 0, 0, 0.8, 0, 1, 0]^T$, then the third, seventh, and ninth elements have 30%, 80%, and 100% damage degree, respectively, whereas other elements are undamaged. By using the real encoding form, we can describe the damage location and degree conveniently and effectively.

The updated velocity and location for the real encoding particle swarm algorithm (RPSO) are expressed in Equations (11) and (12), respectively:

$$v_{id}^{k+1} = \alpha v_{id}^k + c_1 r_1 \times (p_{id}^k - x_{id}^k) + c_2 r_2 \times (p_{gd}^k - x_{id}^k), \tag{11}$$

$$x_{id}^{k+1} = x_{id}^k + v_{id}^{k+1} \quad 1 \le i \le N \quad 1 \le d \le D. \tag{12}$$

Here, α, c_1, and c_2 are constant; r_1 and r_2 are uniformly distributed random numbers between 0 and 1; N is the population size; D is the dimension of particles; x_{id}^k is the current location of the ith particle in the dth dimensional space at step k; p_{id}^k is the personal best location of the ith particle in dth dimensional space at step k; p_{gd}^k is the global best location of the ith particle in the dth dimensional space at step k. $c_1 r_1 \times (p_{id}^k - x_{id}^k)$ denotes that the different elements between the personal best and current locations are exchanged in pairs by

probability c_1r_1 to update the velocity and location of the particles. $c_2r_2 \times (p_{gd}^k - x_{id}^k)$ has a similar meaning.

3.2. RMPSO algorithm

If a particle has found an optimal location via single-swarm PSO, other particles will quickly approach that particle. This phenomenon may result in decreased population diversity. If the current optimal location is a local extreme value, then the particles may no longer search in the solution space; thus, the PSO falls into the local extreme value and then "prematurity" phenomenon occurs. A hierarchical real encoding three-population PSO algorithm, which is based on parallel structure and grade evaluation, is proposed to improve global optimization performance in allusion to these problems. The RMPSO algorithm simulates biogenic accumulation in nature. Three separate species are produced based on different fitness values of particles in the initial stage, including one small-scale elite population with a high matching degree and two large-scale civilian populations with low matching degrees. Three populations exchange particles after certain iterations on the basis of grade evaluation and migration strategy. The idea of the RMPSO algorithm is illustrated in Figure 1.

The key steps of RMPSO are described as follows.

1. Initialize the PSO and divide the particles into three populations. Initialize the velocity and location of particles by real encoding and guarantee that the dimension of each particle is equal to the number

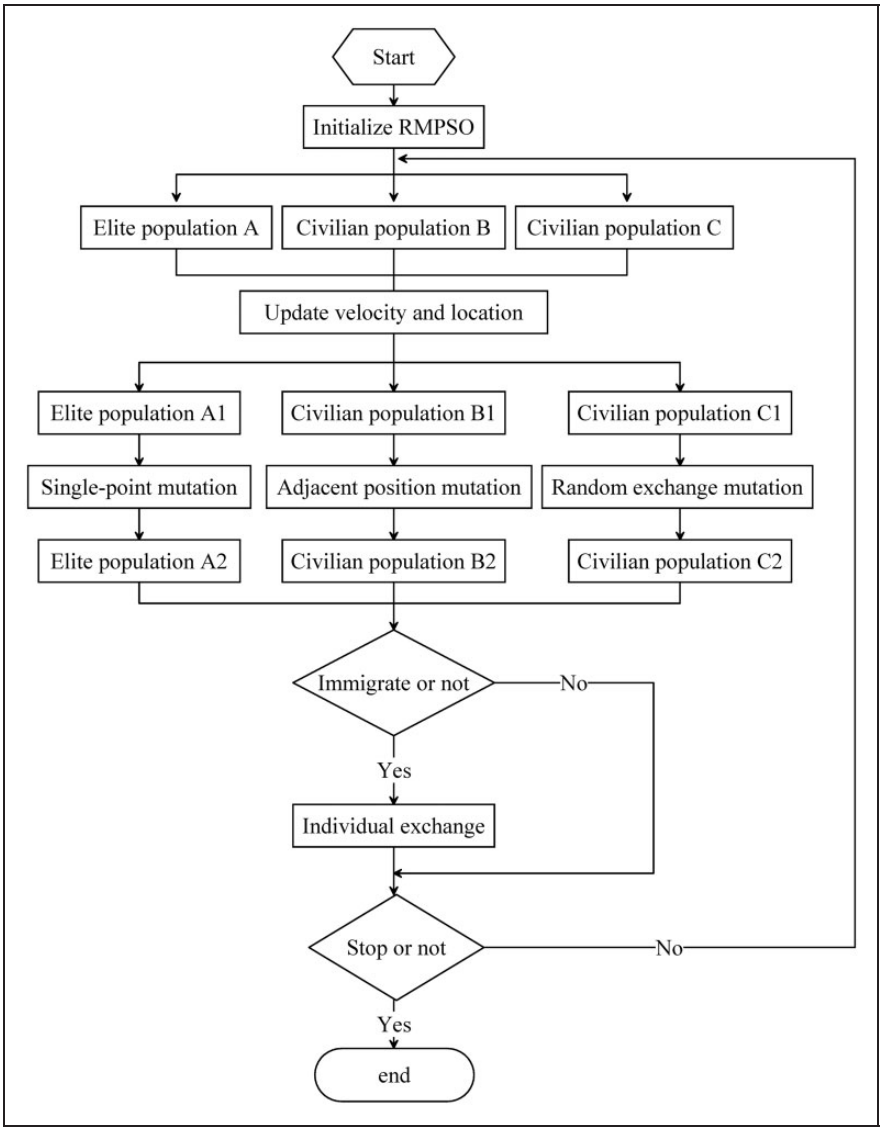

Figure 1. The flowchart of the real encoding multi-swarm particle swarm optimization (RMPSO) algorithm.

of potential damage elements. Evaluate the fitness of initial particles and divide the whole population into three parts, one of which is the small-scale elite population (A) with low fitness values (high matching degree) and the other two are large-scale civilian populations (B and C) with high fitness values (low matching degree). Initialize the iteration times "Iteration" = 1, the maximum iteration times "MaxIter," and the iteration times with the same global best "Samecounter" = 0.

2. Update the velocity and location of each population. Calculate the fitness values of each particle and obtain the "gbest" of each population and "pbest" of each particle according to fitness. Update the velocity and location of each population separately by using Equations (11) and (12) to produce the updated elite population A1 and civilian populations B1, C1.
3. Mutation operator. The mutation operators of the GA are considered high-frequency mutation operators to enhance the global optimization ability of PSO. Firstly, the single-point mutation operator is employed in the elite population to adjust the nonzero dimensions and to search for more accurate damage degrees. The adjacent position mutation operator is applied in civilian population B; that is, random selected dimensions of particles in this civilian population are moved forward or backward to detect the adjacent locations and to ensure the real damage position. Finally, the random exchange mutation operator is applied in civilian population C to speed up the search for the best solution; that is, random selected dimensions are exchanged in pairs. The three mutation operators provide an approach to new solutions without the influence of other particles, thereby improving the population diversity. The fitness values of the particles before and after mutation are compared. The particles with low fitness values (high matching degree) are reserved, and elite population A2 and civilian populations B2, C2 are produced.
4. Verify whether the immigration condition is achieved to complete the individual exchanges of elite and civilian populations. For example, set the immigration frequency $f = 2$ and the number of immigrants $T = 2$. One immigration processing is carried out every two iterations, and two particles with the lowest fitness values (highest matching degree) in each civilian population will immigrate into the elite population, while four particles with highest fitness values (lowest matching degree) in elite population will simultaneously immigrate into the two civilian populations. High-quality particles are selected by immigration operation on the basis of grade evaluation during optimization, and the exchanged particles can be used as "exotic species" to enhance the diversity of population and to avoid trapping into the local optimum.
5. Compare the global best fitness values before and after the update. If the values are the same, one is added to the "Samecounter." If not, the value of "gbest" will be updated, and "Samecounter" will be reset.
6. Stop the iterations if the "Samecounter" achieves a preset value or if the iteration step reaches the maximum. Output the results. If the above requirements are not met, return to step (2).

Each dimension of particles must be ensured to search between 0 and 1. If not, reset these dimensions to 0.

4. Application case

The procedure of the proposed approach for structural damage detection can be summarized in the following steps. To detect the structural damage accurately, secondary development for the FE model was carried out with Matlab software. The RMPSO algorithm was used to update the physical parameter of elements to achieve optimal matching between measured and simulated modal parameters and to obtain the FE model that can reflect the actual structure condition. Figure 2 shows the procedure of the proposed approach.

4.1. Selection of the research object and target modes

The left-hand guide wall structure of Xiangjiaba power station was used to demonstrate the efficiency of the proposed approach in identifying structural damages. The guide wall structure was a 65.75 m high concrete structure. The thickness of the structure was 6.7 m at the crest, and the maximum thickness was 48.2 m at the base. Figure 3 shows the FE model of a concrete guide wall structure section between two structural joints. Eight-node three-dimensional (3D) brick elements were used in the FE model. The density of the concrete material was set at 2400 kg/m^3, the elasticity modulus at 35 GPa (undamaged), and the Poisson's ratio at 0.167. The model had a total of 500 nodes and 420 elements. The hydrodynamic pressure effect was performed by using the added mass to calculate the wet modal parameters of the concrete guide wall structure. Low-frequency modes with high modal participation factors can usually provide sufficient information to describe the dynamic behavior of large structural systems; thus, the first six modes were selected as target modes. Without loss of generality, this paper performed

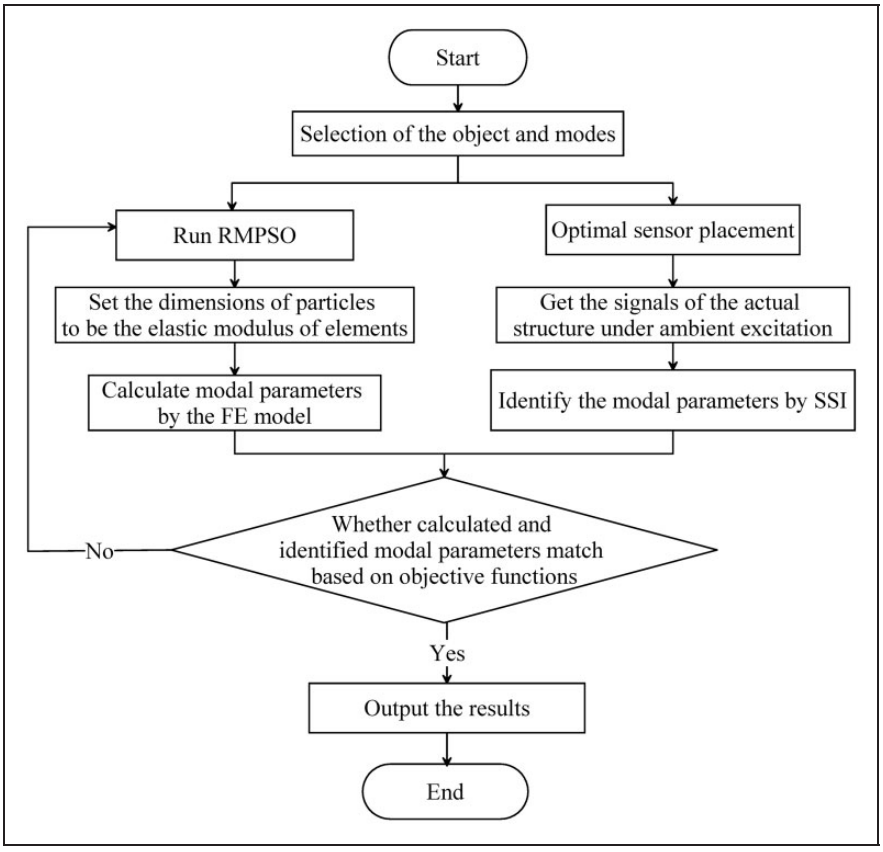

Figure 2. The procedure of the proposed method for damage identification. RMPSO: real encoding multi-swarm particle swarm optimization; FE: finite element; SSI: stochastic subspace identification.

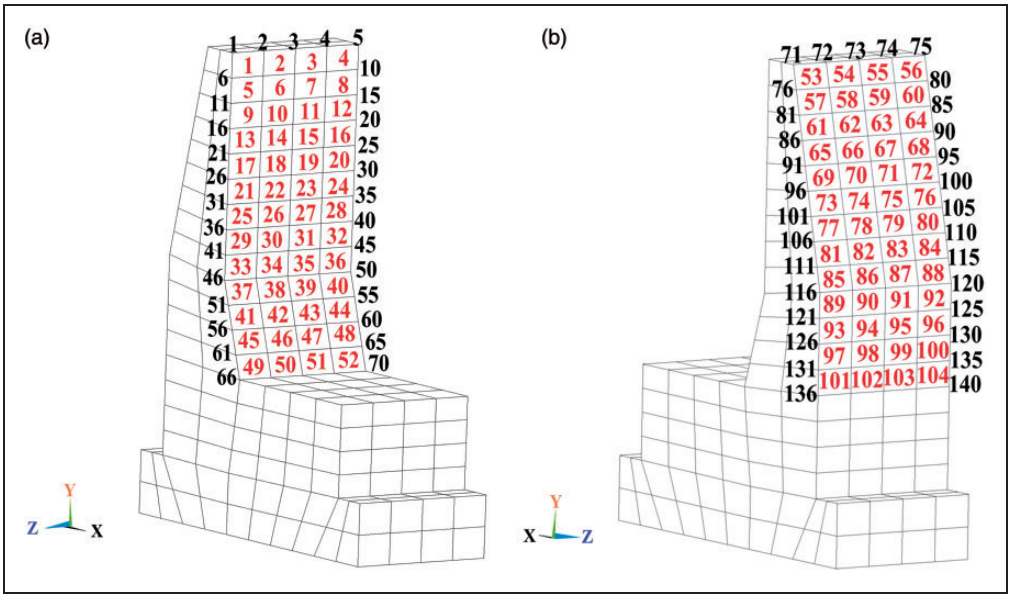

Figure 3. The finite element model of the guide wall structure.

damage detection on the basis of the vibration characteristic of the Y direction. In addition, elements 1–104 (marked red in Figure 3) were selected as potential damage elements, because the stiffness of the cantilever in the concrete guide wall structure was relatively small.

4.2. Optimal sensor placement

The optimal sensor placement is an important tool that can obtain enough modal information, thus ensuring the accuracy of damage detection. Figure 3 shows the candidate nodes numbered 1–140. Table 1 lists the displacement sensor and the strain sensor configurations in the Y direction with 8, 10, 15, and 20 sensors, which were obtained by using a sensor placement method on the basis of information entropy (Papadimitriou et al., 2000).

4.3. Modal parameter identification considering noise

Given the convenience of the multiple-case study, FE model simulation was used to obtain the signals in this study. The noise in measured signals mainly includes the noise of ambient excitation, the noise of sensors, and the noise of the measuring instrument system. The noise from ambient excitation is usually considered as input and not as a noise in the structural measurement. Therefore, we supposed the noise of the measuring instrument system as white noise, which follows the Gaussian distribution. In the FE simulation, the Gaussian white noise was considered as input to simulate ambient excitation and to collect the vibration response of the concrete guide wall structure. The sampling frequency was set at 100 Hz, and the sampling time was 100 s. White noise was added to the measured output, which is given as follows:

$$x_i^Z = x_i + x_{i\max} \times randn \times ns, \tag{13}$$

where x_i refers to the original signal of the ith measured point; x_i^Z refers to the signal with noise; $x_{i\max}$ is the maximum of x_i; *randn* represents the Gaussian white noise, which has an average of 0 and standard deviation of 1; *ns* is the noise level of time history signals. Thus, the standard deviation of the noise is *ns* times the maximum of the time history data, and *ns* is 2% and 5% in this study.

Taking two simultaneous damages (element 9 with 30% damage and element 27 with 50% damage) as an example, Figures 4 and 5 show the displacement and strain time history response signals with 2% noise under ambient excitation, respectively. Figures 6 and 7 show the normalized power spectrums of corresponding signals, from which the first six measured frequencies are 3.13, 9.38, 13.09, 17.38, 21.48, and 22.75 Hz, respectively.

The data-driven stochastic subspace identification method (Basseville et al., 2004; Gontier, 2005) was

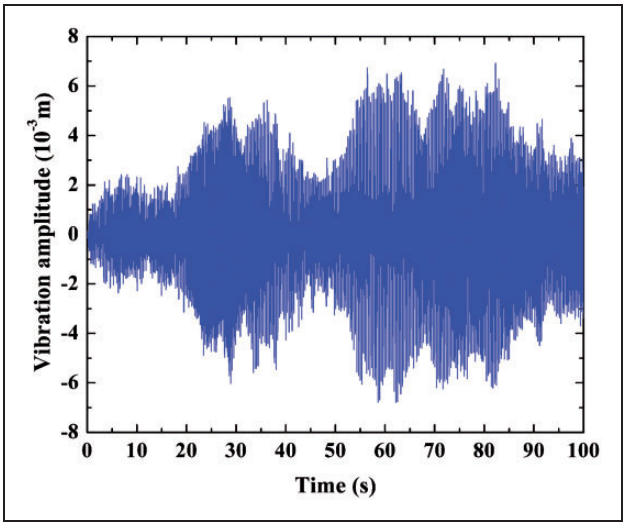

Figure 4. Time history signals of displacement.

Table 1. The schemes of optimal sensor placement.

Sensor type	Number of sensors	Node number
Displacement sensor	8	2, 5, 23, 25, 55, 67, 109, 116
	10	2, 5, 16, 23, 25, 51, 55, 67, 109, 116
	15	2, 5, 10, 16, 23, 25, 35, 51, 55, 61, 67, 85, 109, 116, 120
	20	2, 3, 5, 10, 16, 23, 25, 26, 35, 39, 51, 55, 61, 67, 81, 85, 109, 116, 118, 120
Strain sensor	8	16, 30, 41, 45, 70, 106, 124, 136
	10	10, 16, 30, 41, 45, 70, 105, 106, 124, 136
	15	10, 16, 23, 30, 41, 43, 45, 61, 70, 105, 106, 116, 124, 126, 136
	20	10, 16, 23, 30, 32, 34, 41, 43, 45, 61, 65, 70, 105, 106, 111, 115, 116, 124, 126, 136

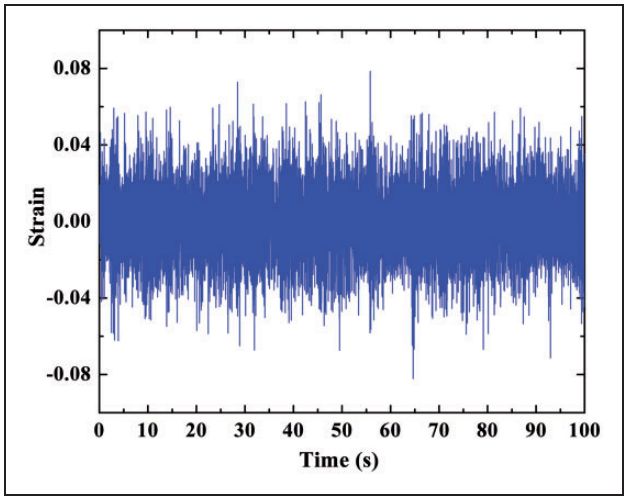

Figure 5. Time history signals of strain.

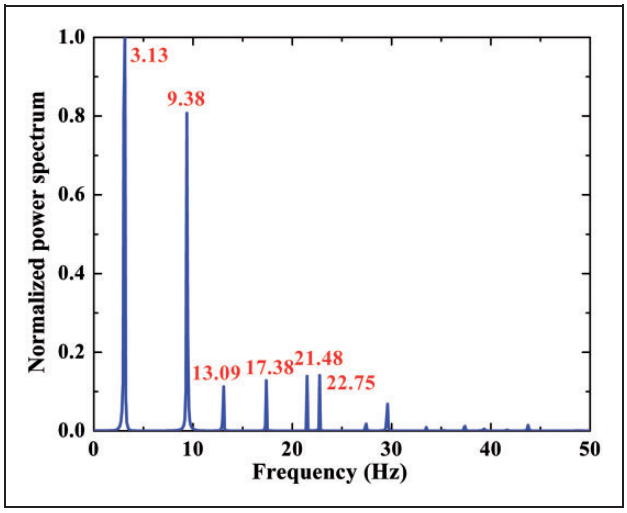

Figure 6. Normalized power spectrums of displacement.

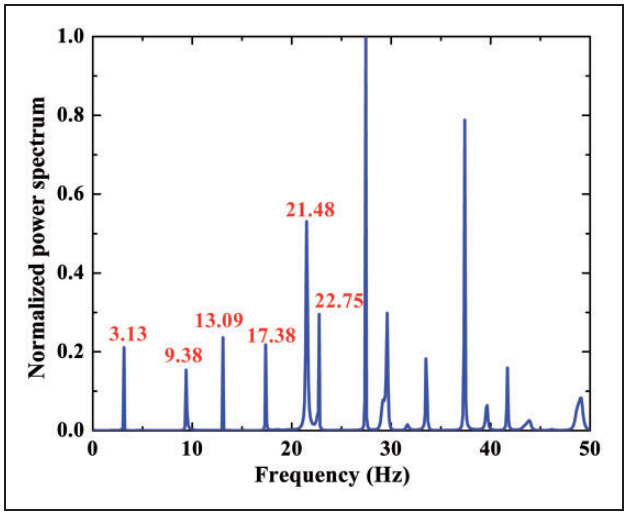

Figure 7. Normalized power spectrums of strain.

adopted to identify the modal parameters (modal frequencies, DMSs, and SMSs) of the concrete guide wall structure under ambient excitation. The frequency stabilization diagram (Zhang et al., 2005) was used to eliminate the false modes. The identified first six frequencies from signals with 2% and 5% noise were compared with the identified frequencies from the original signals, and the average errors were 0.2% and 0.3%, respectively. The identified first six DMSs from signals with 2% and 5% noise were compared with the identified DMSs from the original signals, and the average of the correlation coefficients of modal shapes were 99.7% and 99.4%, respectively. The identified first six SMSs from signals with 2% and 5% noise were compared with the identified SMSs from the original signals, and the average of the correlation coefficients of modal shapes were 99.5% and 99.3%, respectively. The identified modal parameters were used as baseline information, and the intelligent algorithm was used to search for the structural damage model that can match the measured modal information.

4.4. Performance verification of algorithms and fitness functions

In this part, the number of sensors was 20, and two simultaneous damages (element 9 with 30% damage and element 27 with 50% damage) were evaluated without regard to noise. Algorithms can obtain satisfactory results when the damage penalty factor $\gamma = 0.05$.

The four different functions optimized by the RMPSO algorithm were implemented to identify the structural damage detection method. The basic parameters of RMPSO are listed as follows: the dimension of particles was 104, the size of each civilian population was 200, the size of the elite population was 50, α was 0.2, both c_1 and c_2 were 0.5, the immigration frequency was 2, and the number of immigrants was 4. The iteration will be stopped when the flag of the algorithm achieves 50 or when the iteration step reaches 1000. The RPSO algorithm and real encoding genetic algorithm (RGA) were performed and compared with the proposed method to demonstrate the effectiveness of the algorithms. The basic parameters of the RPSO and RMPSO algorithms were basically the same. The parameters of the RGA adopted the definitions in the existing reference (Gomes and Silva, 2008). Each method was carried out 10 times. Figures 8–11 show the best optimization process for three algorithms on the basis of four fitness functions, respectively. According to these figures, the RMPSO algorithm proposed in this study has obvious advantages in optimization efficiency dealing with intelligent damage detection. The RMPSO algorithm not only has fast convergence, but also can achieve the theoretical

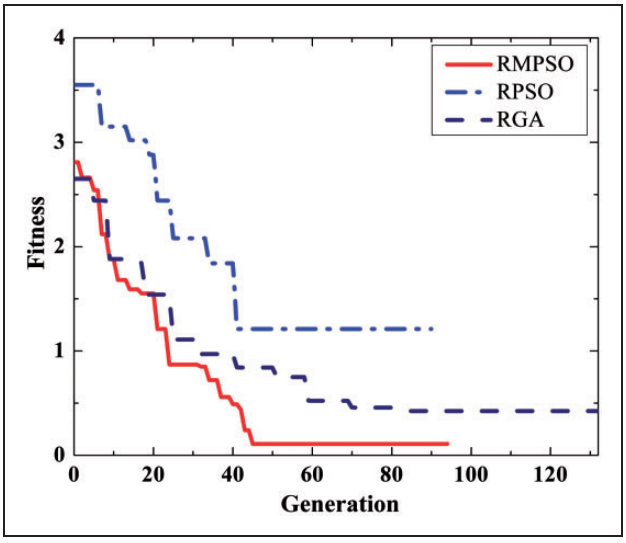

Figure 8. Fitness curves of objective function 1. RMPSO: real encoding multi-swarm particle swarm optimization; RPSO: real encoding particle swarm algorithm; RGA: real encoding genetic algorithm.

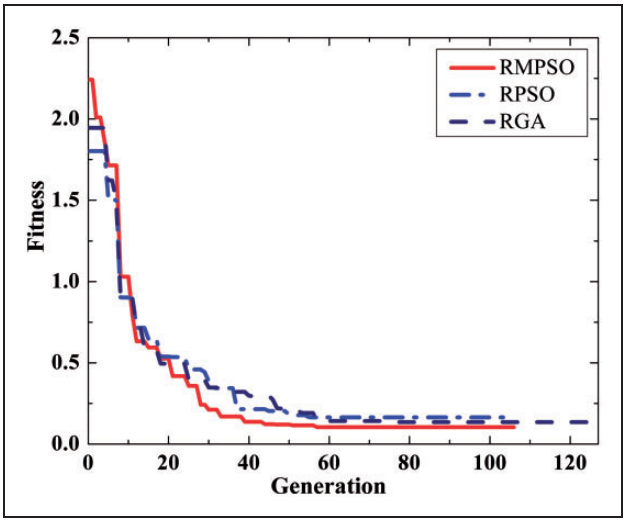

Figure 10. Fitness curves of objective function 3. RMPSO: real encoding multi-swarm particle swarm optimization; RPSO: real encoding particle swarm algorithm; RGA: real encoding genetic algorithm.

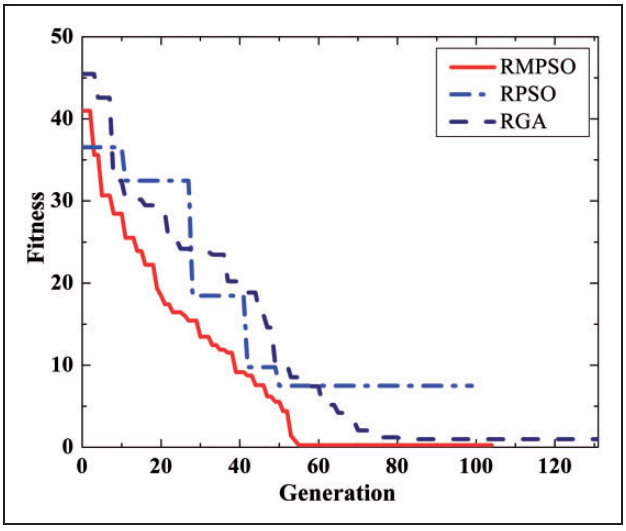

Figure 9. Fitness curves of objective function 2. RMPSO: real encoding multi-swarm particle swarm optimization; RPSO: real encoding particle swarm algorithm; RGA: real encoding genetic algorithm.

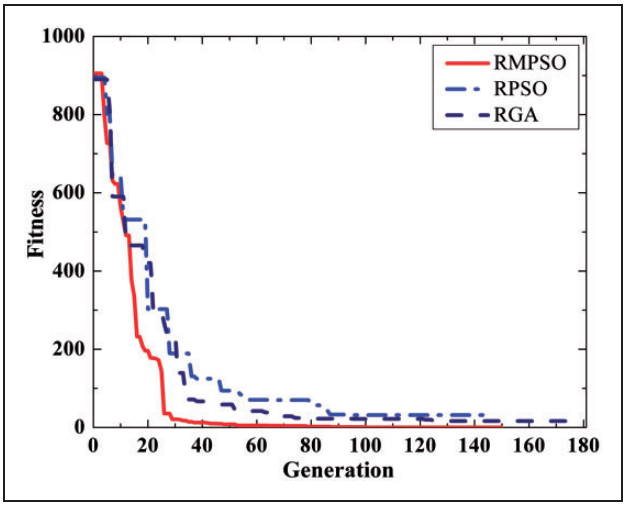

Figure 11. Fitness curves of objective function 4. RMPSO: real encoding multi-swarm particle swarm optimization; RPSO: real encoding particle swarm algorithm; RGA: real encoding genetic algorithm.

optimal solution (0.04). Although the RPSO algorithm has fast convergence, this algorithm decreases easily to the local extreme value. Moreover, the optimization ability of the RPSO algorithm is worse than that of the RMPSO algorithm. The RGA, which is an improvement of the GA, requires more iterative steps compared with the RPSO and RMPSO algorithms. Meanwhile, its optimization results are better than those of the RPSO algorithm, but worse than those of the RMPSO algorithm. Overall, the RMPSO algorithm is an efficient global optimization algorithm that can deal with intelligent damage detection of high dimensions.

Among the fitness functions, the fourth fitness function has the largest distinction degree and the best damage detection capability. The distinction degrees of the first three fitness functions are only about 4, 50, and 2.5, respectively, whereas the distinction degree of the fourth fitness function is almost 1000.

In this paper, we denoted that an element is considered undamaged if the value of its corresponding dimension is not more than 0.02. Figure 12 shows the damage detected by four fitness functions. In this figure, the red arrows direct the real damage locations, and F1–F4 represent the four fitness functions. As shown in Figure 12, only the fourth fitness function detected the damage locations and degrees correctly, whereas the results of the first three fitness functions were not satisfactory. In the next section, we will discuss

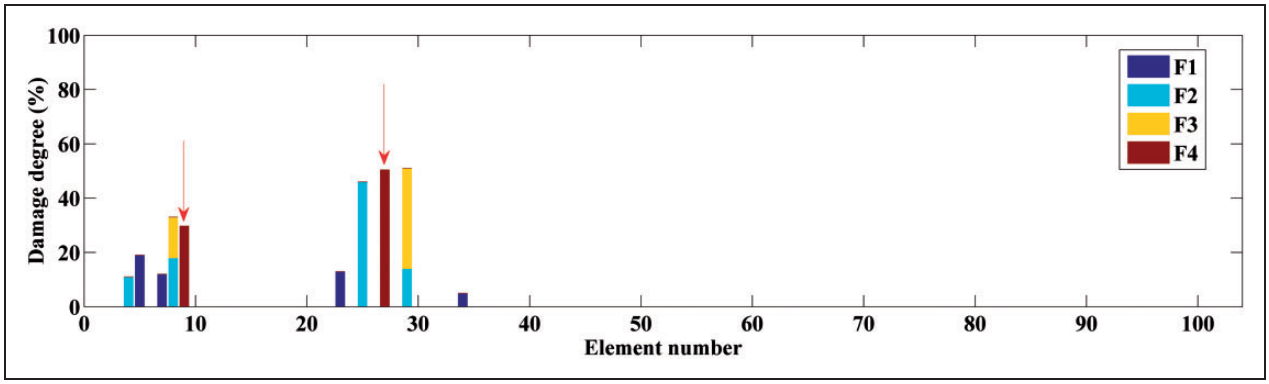

Figure 12. Damage detected by four fitness functions.

Table 2. Damage detected with different numbers of sensors and noise levels.

Case	Number of sensors	Real		Detected (no noise)		Detected (2% noise)		Detected (5% noise)	
		Location	Degree (%)	Location	Degree (%)	Location	Degree (%)	Location	Degree (%)
1	8	18	50	18	47	18	45	18	43
	10	18	50	18	46	18	46	18	45
	15	18	50	18	49	18	50	18	49
	20	18	50	18	51	18	49	18	50
2	8	64	20	59 62	15 13	55 59	18 25	63 72	17 12
	10	64	20	64	18	64	21	64	22
	15	64	20	64	21	64	20	64	19
	20	64	20	64	20	64	19	64	20
3	8	10 27	20 10	7 19 35	18 13 5	15 43	17 33	9 25 31	10 9 16
	10	10 27	20 10	10 27	17 12	10 27	18 8	10 26	22 13
	15	10 27	20 10	10 27	21 10	10 27	20 9	10 27	19 9
	20	10 27	20 10	10 27	20 10	10 27	20 10	10 27	19 10
4	8	34 70	70 40	26 35 82	51 29 18	30 69 74	53 16 22	21 41 60 78	24 13 35 29
	10	34 70	70 40	31 65 72	65 22 13	29 38 70	28 35 32	29 39 70	25 40 33
	15	34 70	70 40	34 70	67 39	34 70	66 41	34 70	68 36
	20	34 70	70 40	34 70	69 39	34 70	68 40	34 70	69 37
5	8	2 23 99	20 50 80	1 23 97	10 42 85	1 23 62 97	8 54 14 63	3 20 87	16 43 69
	10	2 23 99	20 50 80	2 21 101	18 53 71	3 24 99	17 53 85	3 19 77 102	13 14 36 51
	15	2 23 99	20 50 80	2 23 98	22 45 84	3 23 70 103	26 39 10 79	5 25 39 91	13 54 22 63
	20	2 23 99	20 50 80	2 23 99	18 51 80	2 23 99	19 53 77	2 23 99	17 53 79
6	8	13 82 104	70 60 50	13 90	88 67	14 77 87 100	71 12 23 65	9 78 100	78 41 39
	10	13 82 104	70 60 50	13 18 74 104	66 25 14 47	17 82 102	68 49 36	17 82 102	65 52 43
	15	13 82 104	70 60 50	13 82 104	66 54 57	13 30 80 104	68 15 43 38	13 31 84 104	67 35 42 46
	20	13 82 104	70 60 50	13 82 104	68 60 49	13 82 104	67 60 50	13 82 104	70 56 49

the fourth fitness function optimized by the RMPSO algorithm.

4.5. Results

Multiple damage cases with different numbers of sensors and noise levels were simulated. The damage cases include single damage, two simultaneous damages, and three simultaneous damages; each damage case has two conditions. The RMPSO algorithm was used to optimize the fourth objective function (the uniform distribution of the ratios of the measured and simulated SMSs). Satisfactory results with no noise, 2% noise, and 5% noise were achieved when the damage penalty factors were 0.05, 0.08, and 0.10, respectively.

Table 2 summarizes the damage detected in each case. In the single damage case, it is possible to locate and quantify the damage correctly by measuring only 10 DOFs (7.1% of the total *Y*-DOFs). The method requires more sensors when the number of damage locations is increased. For two simultaneous damages, the method needs at least 15 DOFs (10.7% of the total *Y*-DOFs), and the three simultaneous damages require at least 20 DOFs (14.3% of the total *Y*-DOFs). The number of DOFs required depends on the structure and complexity of the damage situation that needs to be detected. Noise influences damage detection, such as in Case 6. The results obtained by using 15 sensors are different whether noise is considered or not.

5. Conclusion

This study proposed a new damage detection method for large structures employing the RMPSO algorithm and the fitness function evolved from strain modes to find an optimal match between measured and simulated modal parameters and to obtain the actual structure condition. The proposed method requires only low-frequency and incomplete modes; thus, this method is highly suitable for the nondestructive dynamic damage detection of large structures under ambient excitation. A concrete guide wall structure was used to verify the approach. The following conclusions are derived.

1. The RMPSO algorithm tends to the global optimum quickly and shows good convergence during algorithm validation. The RMPSO algorithm is proved to be a more efficient global optimization algorithm compared with the existing RPSO algorithm and RGA in dealing with intelligent damage detection of high dimensions.
2. Four objective functions were compared, and the results show that the uniform distribution of the ratios of measured and simulated SMSs are more effective in detecting structural damage compared with the other objective functions.
3. The new damage detection method was used to update the parameters of the FE model, search the optimal matching with actual parameters of structural damage, and detect the damage with multiple damage scenarios. Results show that locating and quantifying the damage correctly by using only 10 DOFs is possible in single damage cases. For two simultaneous damages, the method requires at least 15 DOFs, whereas the three simultaneous damage cases require at least 20 DOFs. Noise also has an influence on damage detection. The number of sensors required depends on the structure, the complexity of the damage situation, and the noise of the measured situation.

The proposed damage detection method can effectively detect the locations and degrees of damage in different damage cases and can be promoted and applied in many types of large structures.

Acknowledgments

The authors are most grateful for the kind assistance of the editors of *Journal of Vibration and Control*, and for the constructive suggestions from the anonymous reviewers, all of which have led to the making of several corrections and have greatly aided us to improve the presentation of this paper.

Funding

This work was supported by the China National Funds for Innovative Research Groups of the National Natural Science Foundation of China (grant number 51021004), the Communication Research Item for the West Area, Ministry of Communications (grant number 2009328000084), the Tianjin Research Program of Application Foundation and Advanced Technology (grant number 12JCQNJC04600), the National Natural Science Foundation of China (grant number 50909072), and the Project supported by the National Natural Science Foundation of China (grant number 51209158).

References

Basseville M, Mevel L and Goursat M (2004) Statistical model-based damage detection and localization: subspace-based residuals and damage-to-noise sensitivity ratios. *Journal of Sound and Vibration* 275(3–5): 769–794.

Cerri MN and Vestroni F (2003) Use of frequency change for damage identification in reinforced concrete beams. *Journal of Vibration and Control* 9(3–4): 475–491.

Doebling SW, Farrar CR and Prime MB (1998) A summary review of vibration-based damage identification methods. *Shock and Vibration Digest* 30(2): 91–105.

Fritzen CP and Jennewein D (1998) Damage detection based on model updating methods. *Mechanical Systems and Signal Processing* 12(1): 163–186.

Gomes H and Silva N (2008) Some comparisons for damage detection on structures using genetic algorithms and modal sensitivity method. *Applied Mathematical Modelling* 32(11): 2216–2232.

Gontier C (2005) Energetic classifying of vibration modes in subspace stochastic modal analysis. *Mechanical Systems and Signal Processing* 19(1): 1–19.

Guo HY and Li ZL (2012) A two-stage method for damage detection using frequency responses and statistical theory. *Journal of Vibration and Control* 18(2): 191–200.

He HX and Yan WM (2007) Structural damage detection with wavelet support vector machine: Introduction and applications. *Structural Control and Health Monitoring* 14(1): 162–176.

He R and Hwang S (2006) Damage detection by an adaptive real-parameter simulated annealing genetic algorithm. *Computers and Structures* 84(31–32): 2231–2243.

Hera A and Hou ZK (2004) Application of wavelet approach for ASCE structural health monitoring benchmark studies. *Journal of Engineering Mechanics-ASCE* 130(1): 96–104.

Hester D and Gonzalez A (2012) A wavelet-based damage detection algorithm based on bridge acceleration response to a vehicle. *Mechanical Systems and Signal Processing* 28((SI)): 145–166.

Huang NE and Shen Z (1998) The empirical mode decomposition and the Hilbert spectrum for nonlinear and non-stationary time series analysis. In: *Proceedings of the Royal Society of London*. Series A, 454, pp.903–995.

Kennedy J and Eberhart RC (1995) Particle swarm optimization. In: *Proceedings of the IEEE conference on neural networks*, Vol. 4, pp. 1942–1948.

Li XY and Law SS (2010) Matrix of the covariance of covariance of acceleration responses for damage detection from ambient vibration measurements. *Mechanical Systems and Signal Processing* 24(4): 945–956.

Li YY, Cheng L, Yam LH, et al. (2002) Identification of damage locations for plate-like structures using damage sensitive indices: Strain modal approach. *Computers and Structures* 80(25): 1881–1894.

Mares C and Surace C (1996) An application of genetic algorithms to identify damage in elastic structures. *Journal of Sound and Vibration* 195(2): 195–215.

Meruane V and Heylen W (2011) An hybrid real genetic algorithm to detect structural damage using modal properties. *Mechanical Systems and Signal Processing* 25(5): 1559–1573.

Minakuchi S, Okabe Y, Mizutani T, et al. (2009) Barely visible impact damage detection for composite sandwich structures by optical-fiber-based distributed strain measurement. *Smart Materials and Structures* 18(8): 1–9.

Papadimitriou C, Beck JL and Au SK (2000) Entropy-based optimal sensor location for structural model updating. *Journal of Vibration and Control* 6(5): 781–800.

Parka JH, Kim JT, Hong DS, et al. (2009) Sequential damage detection approaches for beams using time-modal features and artificial neural networks. *Journal of Sound and Vibration* 323(1–2): 451–474.

Qian JR, Ji XD and Zhang WJ (2008) Damage detection test of a substructure model of the National Swimming Center. *Science in China Series E-Technological Sciences* 51(7): 940–948.

Song HZ, Zhong L and Han B (2006) Structural damage detection by integrating independent component analysis and support vector machine. *International Journal of Systems Science* 37(13): 961–967.

Tang JP, Chiou DJ, Chen CW, et al. (2010) A case study of damage detection in benchmark buildings using a Hilbert–Huang Transform-based method. *Journal of Vibration and Control* 17(4): 623–636.

Tsuda H, Toyama N, Urabe K, et al. (2004) Impact damage detection in CFRP using fiber Bragg gratings. *Smart Materials and Structures* 13(4): 719–724.

Vakil-Baghmisheh MT, Peimani M, Sadeghi MH, et al. (2008) Crack detection in beam-like structures using genetic algorithms. *Applied Soft Computing* 8(2): 1150–1160.

Wu X, Ghaboussi J and Garrett JH (1992) Use of neural networks in detection of structural damage. *Computers and Structures* 42(5): 649–659.

Zhang Y, Zhang Z, Xu X, et al. (2005) Modal parameter identification using response data only. *Journal of Sound and Vibration* 282(1–2): 367–380.